Journal of Materials Chemistry C

PAPER

View Article Online
View Journal

Cite this: DOI: 10.1039/c9tc02311a

Highly stretchable electromagnetic interference (EMI) shielding segregated polyurethane/carbon nanotube composites fabricated by microwave selective sintering†

Dong Feng, Dawei Xu, Qingqing Wang and Pengju Liu *

Received 1st May 2019,
Accepted 24th May 2019

DOI: 10.1039/c9tc02311a

rsc.li/materials-c

The formation of a segregated structure in conductive polymer composites (CPCs) is one of the most promising strategies for achieving good electrical conductivity and electromagnetic interference (EMI) shielding performance. Nevertheless, the segregated CPCs usually suffer from deteriorated mechanical properties due to the limited interfacial interaction between polymer granules hindered by the conductive layer. We propose a novel sintering method utilizing the intense selective heating of conductive fillers upon microwave irradiation, which shows obvious advantages over conventional compression molding (CM). To do so, carbon nanotubes (CNTs) were used as microwave absorbers in the thermoplastic polyurethane (TPU) media. Upon irradiation, CNTs were responsible for a local temperature increasing spot on the surface of TPU granules, promoting the molecular diffusion among TPU only in the interface region without damaging the segregated structure. In this way, the elongation at break of the as-prepared TPU/CNT composites reached 350%, approximately ten times higher than that of the composites prepared by the conventional CM. Meanwhile, the microwave sintering (MS) composites showed comparable electrical conductivity and EMI shielding effectiveness (SE) to the CM samples. Our current efforts provide an insight into the development of a highly stretchable EMI shielding material *via* the "green" method.

1. Introduction

Conductive polymer composites (CPCs) have attracted increasing academic and industrial attention owing to their light weight, low cost, good processability and tunable electrical conductivity.[1–5] In view of these characteristics, CPCs show significant advantages over conventional metal-based materials in the application of microwave absorption, *e.g.*, shielding materials for protection of electronic devices, reduction in electromagnetic exposure, and camouflage materials for radar and defense projects.[6–9] It has been well established that the the EMI SE of CPCs is strongly associated with their electrical conductivity.[10] To achieve the target EMI SE value (>20 dB) for commercial use, the conductive filler loading is typically high for the filler particle incorporation-mixing process (>10 wt%), which in turn will always bring adverse effects, *i.e.*, high cost, poor processability and mechanical properties.[11–13]

The formation of a segregated structure by incorporating a small amount of highly conductive nanoparticles in a polymer matrix, like carbon black (CB), carbon nanotubes (CNTs) or graphene,[14] is found to be an effective way to fabricate CPCs with improved electrical conductivity over traditionally randomly distributed composites.[15–17] The conductive paths are readily formed and connected to construct a dense network, thus significantly lowering the percolation threshold of CPCs. For instance, the CB-based acrylonitrile–butadiene–styrene (ABS) composites with a segregated network structure showed an ultralow percolation of 0.0054 vol%.[18] The electrical conductivity of the segregated polycarbonate/graphene composites achieved was 0.512 S cm^{-1} when 2.2 vol% graphene was assembled on the polycarbonate microsphere surfaces through an emulsion mixing method.[19] A comparative study of the segregated and randomly distributed CNT/poly(phenylene sulfide) composites revealed that the EMI SE of the former (49.6 dB) was two times higher than that of the latter (24.9 dB) at a CNT loading of 5 wt%.[17]

However, it should be noted that although considerable electrical conductivity and EMI shielding performance are easily achieved, deteriorated mechanical strength will occur, thus severely limiting the application of segregated CPCs. Considering the manufacturing process of the segregated CPCs, the inferior mechanical performance is mainly due to the fusion defects caused by the restricted molecular diffusion

State Key Laboratory of Polymer Materials Engineering, Polymer Research Institute of Sichuan University, Chengdu 610065, China. E-mail: sculpj@163.com

† Electronic supplementary information (ESI) available. See DOI: 10.1039/c9tc02311a

during the hot compression molding of the coated polymer granules. Besides, the unavoidable agglomeration of the rigid conductive fillers may form micro-defects (*i.e.*, micro-voids) along the conductive paths, also leading to poor mechanical performance.[20] Unfortunately, relatively few studies have been devoted to enhancing the mechanical performance of the segregated CPCs. Currently, concerns have been provided either by incorporating the third component as an interfacial binder[21,22] or applying high pressure molding to promote the inter-diffusion of molecular chains across the granule boundaries.[20] Despite these efforts, drawbacks still exist, including complicated crafts, harsh processing conditions, and high requirements for equipment. More importantly, for a conventional heating mode, the heat transfer from the heat source to composites requires much heating time (especially for the large and complex shaped products), thus the formed non-uniform temperature distribution is a disadvantage in the construction of a high-quality conductive network. Therefore, developing an efficient strategy to enhance the mechanical properties of the segregated CPCs is still a great challenge and urgently needed.

Microwave (MW) is a form of electromagnetic radiation with frequencies ranging from 300 MHz to 300 GHz, and it can cause heating when materials absorb MW radiation. MW heating is a volumetric heating process which is efficient, energy saving, clean, and environment-friendly.[23] More importantly, MW shows the selective heating behavior for different materials depending upon their electromagnetic characteristics. In general, thermoplastic polymers are transparent to MW, while the conductive fillers, especially CNTs are excellent MW absorbents and can be heated vigorously upon MW irradiation.[24,25] Taking advantage of the distinctive heating behavior between the thermoplastic polymers and conductive fillers, CNTs can serve as "solder" to locally melt and weld the polymer matrix upon MW irradiation. This MW sintering approach has been used to prepare high-strength polymer composites,[26–28] three-dimensional (3D)-printed parts,[29] and other functional composites.[30–32]

To address the above issues, we proposed a novel approach to fabricate the segregated TPU/CNT composites by combining ball-milling and MS technology. Firstly, ball-milling was used to selectively distribute the CNTs onto the surface of TPU granules to obtain the coated TPU/CNT powder, and followed by MW irradiation to sinter the coated powder into three-dimensional TPU/CNT parts with a segregated structure. The obtained TPU/CNT composites in this study feature excellent mechanical strength, high electrical conductivity and superb EMI SE, and the facile technology proposed in our study may have great potential to construct a segregated conductive network in various types of polymers.

2. Experimental

2.1. Materials

TPU particles (Bayer 870) were supplied by Suyu plastic Co., Ltd. Carbon nanotubes (CNTs, NC7000) with an average diameter of 9.5 nm and a length of 1.5 μm were obtained from Nanocyl S.A., Belgium.

2.2. Fabrication of the TPU/CNT composites

The fabrication of the segregated TPU/CNT composites is shown in Fig. 1. Initially, TPU powder was mixed with CNTs (0.1 wt%, 0.5 wt%, 1.0 wt%, 3.0 wt% and 5.0 wt%) in a ball milling machine (QM-3SP4, Nanjingnanda instrument Co., Ltd, China) at 350 rpm for 1 h to obtain CNT coated TPU complex powder. Then, the complex powders were filled into our self-designed Teflon mold (shown in Fig. S1, ESI†), followed by placing it in a microwave oven *via* microwave sintering (MS). After a certain period of MS, an appropriate compressive stress was applied to achieve desired welding between powders. The obtained composites with different CNT contents were denoted as $MS_{0.1}$, $MS_{0.5}$, $MS_{1.0}$, $MS_{3.0}$, $MS_{5.0}$. To make sure a high quality sintering behavior, specifically, the complex TPU/CNT powders with 0.5, 1.0, 3.0 and 5.0 wt% CNTs were sintered at 300 W for 45, 15, 10 and 8 s, respectively, while $MS_{0.1}$ was sintered at 750 W for 45 s, these conditions were chosen after many trials. Based on the literature,[33,34] we assumed that the electric field was maximum at the center of the MW cavity and therefore the samples received a uniform field. To place the samples in the middle of the microwave cavity, a Teflon stand was used. In contrast, the segregated TPU/CNT composites by compression molding (CM, molded at 55 °C and 10 MPa for 10 min) were also prepared (samples denoted as $CM_{0.1}$, $CM_{0.5}$, $CM_{1.0}$, $CM_{3.0}$, $CM_{5.0}$) according to a previous study.[35]

2.3. Scanning electron microscopy (SEM) observation

The micro morphologies of the CNT coated TPU complex powder and the cryo-fractured TPU/CNT composites prepared in liquid nitrogen were observed using an Inspect F SEM

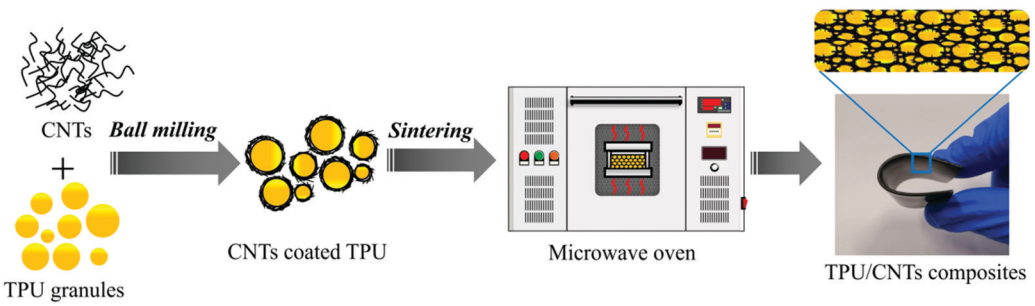

Fig. 1 Schematic of procedure for fabricating TPU/CNT composites *via* MS.

instrument (FEI Co., Ltd, USA). The fractured surfaces were sputtered with gold in a vacuum and the test was performed at 0.5 Torr and 20 kV.

2.4. Optical microscopy (OM) observation

For OM measurements, the TPU/CNT composites were cut into a 30 μm-thick film using a microtome and the film was observed using a Leica DM2500P optical microscope (OM) connected with a pixel camera (Leica, USA). The thin TPU/CNT film tends to curl, and must be sandwiched between two glass slides to remain flat during the OM observation. Silicone oil with high viscosity is first dropped on the glass slide, promoting the thin film to fully spread on the substrate.

2.5. Mechanical property test

Tensile and compression strength of TPU/CNTs were tested using an Instron 5567 (Instron Co., Ltd, United States). A square sample with 40 × 10 × 2 mm dimension for tensile testing was cut according to GB/T 9641-1988/ISO 1926–1979, and the crosshead speed was 50 mm min^{-1}. A cylindrical sample with a diameter of 15 mm and a height of 10 mm was used for compression testing according to GB/T 8813-2008/ISO 844:2004, and the crosshead speed was 5 mm min^{-1}.

2.6. Electrical property test

For the electrical resistance test, samples were cut into disc sheets with a diameter of 15 mm and a height of 2 mm. A fourpoint probe instrument (RK-FA, Ningbo Ruikeweiye instrument Co., Ltd, China) was used to measure the resistance, and five measurements were performed for each sample and the average was obtained. It should be noted that the electrical resistance of TPU/CNTs with 0.06 vol% CNTs was measured using a digital multimeter (Fluke 8062A), and the corresponding electrical conductivity was calculated through the equation $\sigma = L/(S \times R)$, where σ and R represent the electrical conductivity and electrical resistance, respectivey and L and S represent the length and cross-sectional area of the disc sheet, respectively.

2.7. EMI shielding test

EMI shielding measurement was performed by using an Agilent N5230 vector network analyzer (USA), with the APC-7 connector as a coaxial test cell. The scattering parameters (S_{11}, S_{12}, S_{21}, S_{22}) in the X-band (8.2–12.4 GHz) were recorded to calculate the reflected power (R), transmitted power (T), absorbed power (A), EMI SE (SE_T), microwave reflection (SE_R) and microwave absorption (SE_A) based on the eqn (1)–(4).[36]

$$R = |S_{11}|^2 = |S_{22}|^2, \quad T = |S_{12}|^2 = |S_{21}|^2 \tag{1}$$

$$SE_R = 10\log\left(\frac{1}{1-R}\right) = 10\log\left(\frac{1}{1-|S_{11}|^2}\right) \tag{2}$$

$$SE_A = 10\log\left(\frac{1-R}{T}\right) = 10\log\left(\frac{1-|S_{11}|^2}{|S_{21}|^2}\right) \tag{3}$$

$$SE_T = SE_R + SE_A = 20\log(S_{21}) \tag{4}$$

3. Results and discussion

3.1. Microstructure and morphology

Ball milling is a common grinding method, which has been widely used to enhance the dispersion of nanofillers in a polymer matrix.[37] The structure and morphology of the fillers can be controlled by changing the applied energy and time. Fig. 2a showed the SEM morphology of the TPU/CNT complex granules, revealing an average particle size of 250 μm after the ball mixing process. At higher magnification (Fig. 2a, inset image), plenty of CNTs were uniformly adhered to the surface of TPU granules, which is favorable for the establishment of a conductive network. To identify the characteristics of the segregated conductive CNT pathways, the fractured surfaces of the $CM_{5.0}$ (Fig. 3b) and $MS_{5.0}$ (Fig. 3d) samples were observed, where the CNTs are preferentially located at the grain boundary and showed a typical segregated structure. As reported in a previous study,[38,39] the fracture surface of $CM_{5.0}$ showed an obvious inter-bead bonding behavior, due to the poor binding force among the complex granules. However, the broken behavior of our MS sample is almost intra-bead bonding mechanism, suggesting a strong local sintering quality and an improved interfacial adhesion *via* our microwave sintering procedure. Besides, the interfacial regions of $CM_{5.0}$ (Fig. 2c) and $MS_{5.0}$ (Fig. 2e) at higher magnification were observed to manifest a detailed microstructure in the segregated composites. CNTs are preferentially located at the grain boundary, demonstrating that the CNTs are indeed prohibited from migrating into the interior of the TPU domains. Thus the obvious micro-voids and relatively large gaps among the TPU regions can be observed from Fig. 2c, leading to the interfacial flaws and poor interfacial interaction. In contrast, as shown in Fig. 2e, the interstices of the enriched CNTs of our MS composites became much smaller, and the strong diffusion between the neighboring TPU regions occurred in the interface area. This could be attributed to the local high-temperature spots caused by microwave-irradiated CNTs, allowing the CNTs more liable to be embedded in TPU domains, instead of forming the

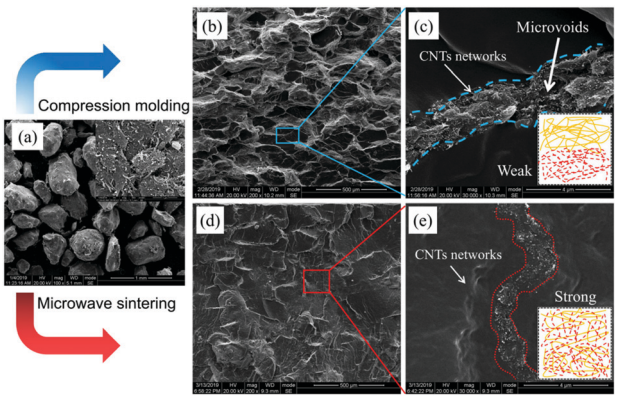

Fig. 2 SEM images of (a) TPU/CNT complex granules (inset shows the magnified image); (b) the fractured surface of the $CM_{5.0}$ composite; (c) the magnified SEM image of (b); (d) the fractured surface of the $MS_{5.0}$ composite; (e) the magnified SEM image of (d).

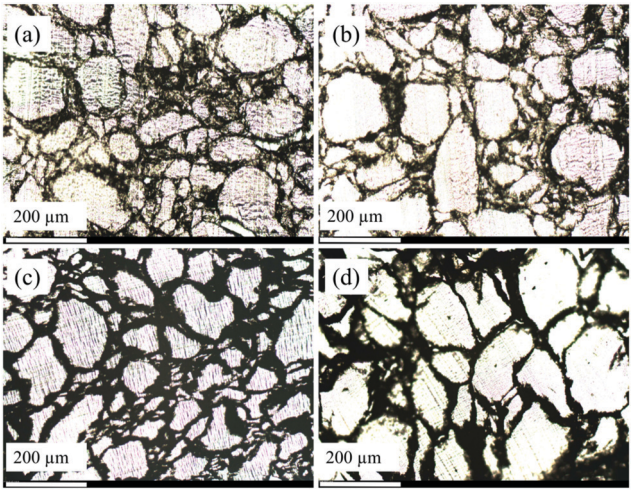

Fig. 3 OM images of the TPU/CNT composites (a) $MS_{1.0}$; (b) $CM_{1.0}$; (c) $MS_{5.0}$ and (d) $CM_{5.0}$.

barrier preventing the TPU chain diffusion. Therefore, the mechanical strength of our MS sample appears to be higher than that of the CM counterpart, and a comparison of tensile strength is displayed and discussed as follows.

The morphology of the TPU/CNT composites prepared by MS and CM was further studied *via* the OM observation to provide an intuitive insight into the segregated structure, and the results are shown in Fig. 3. Coinciding with the SEM observations, a typical segregated structure is observed for both the MS and CM composites, in which the CNTs were selectively distributed at the interface of the adjacent TPU granules regardless of the CNT content. As the CNT content increases from 1.0 wt% (Fig. 3a and b) to 5.0 wt% (Fig. 3c and d), the conductive pathways (black line) composed by incomputable CNTs become thicker, indicating the perfection of the conductive network. The corresponding OM results reveal that MS is a facile yet highly efficient approach for the construction of a 3D conductive network in TPU domains. The formation of a segregated CNT network is beneficial for achieving both outstanding electrical conductivity and EMI shielding performance of the TPU/CNT composites.

3.2. Mechanical properties

A systematic comparison of mechanical properties of MS and CM samples is shown in Fig. 4. Fig. 4a shows the comparison of the tensile strength of MS and CM samples with various CNT contents. In agreement with the published data,[40] the tensile strength of the CM samples significantly decreases with increasing CNT content, such as from $CM_{0.1}$ of 8.0 MPa to $CM_{5.0}$ of 4.8 MPa. This is due to the thicker interfacial CNT layers which severely hinder the chain diffusion between the neighboring TPU granules. In contrast, a significant enhancement in tensile strength of the TPU/CNT composites was obtained through MW sintering, particularly for the segregated composites with a high CNT content. For example, $MS_{5.0}$ showed an enhanced tensile strength of 11.5 MPa, more than twice as high as $CM_{5.0}$ (4.8 MPa). The tensile strength of the MS composites with over 0.5 wt% CNTs was much higher than that of pure TPU prepared by compression molding, indicating a reinforcing effect of CNTs for the TPU matrix. Apart from the obtained improvement in tensile strength, an amazing increase in the elongation at break was observed for MS samples. The elongation at break of $MS_{0.5}$ reached 350%, over ten times higher than that of $CM_{0.5}$. Even for the TPU/CNT sample with high CNT loading fractions, the enriched CNTs promoted the strong interfacial adhesion between the TPU granules under MW irradiation. The photograph of the stretching $MS_{5.0}$ sample at a strain of 250% was shown in Fig. S2 (ESI†), clearly demonstrating the highly enhanced stretchability of the MS composites. Fig. 4c also shows the tensile moduli of the MS composites with various CNT loadings. The modulus of the MS composites increased with an increase in the CNT content from 0.1 to 0.5 wt%, and reached a saturation value of around 45 MPa at a high loading content.

Based on an in-depth understanding of the MW sintering process, the simultaneous enhancement in strength and toughness could be attributed to the CNT "welding" mechanism, in which the irradiated CNTs (act as hot spot) were embedded in TPU granules, thus ensuring a good interfacial interaction (CNTs also act as a connecting agent between the neighboring granules). But for the conventional CM strategy, the segregated structure can only be fixed in a high-viscosity polymer matrix, thus requiring a relatively low shaping temperature leading to the poor interfacial adhesion and unavoidable micro-voids.

In addition, stretching-recovery cyclic tests were conducted to further demonstrate the mechanical stability of the MS composites. Fig. 4d shows the results of the cyclic tensile tests for the $MS_{5.0}$ sample. The maximum tensile stress at a strain of 30% only decreased from 11.9 to 10.6 MPa even after 500 stretching cycles, as compared to the first cycle. We also recorded the compression behavior of the MS composites during the cyclic loading–unloading process. From Fig. 4e, the compression strength and modulus of $MS_{5.0}$ increased significantly with an increase in the applied strain from 10 to 50%. Fig. 4f shows the cyclic stress–strain curves at various compressive strains of 10%, 30% and 50%, respectively. At all compressive strains, the first loading cycle showed the highest stress, such as 12.0 MPa at 50% strain, and the stress decreased gradually in the second loading cycle and remained steady in the subsequent cycle with the same strain, suggestive of a good reversibility and reproducibility in terms of outer loading pressure. Based on the above results, the mechanically strong TPU/CNT composites fabricated by our MS techniques show great promise to serve as structural materials for severe stress applications.

3.3. Electrical conductivity performance

Fig. 5 shows the electrical conductivity of MS and CM composites as a function of CNT volume fraction. It can be seen that a dramatic increase in electrical conductivity was observed with the CNT content increasing from 0.06 to 2.94 vol%. At a given CNT content, the MS samples exhibited a comparable electrical conductivity as the CM samples, for instance, the electrical conductivity at 1.74 vol% of CNT content is 7.7 S m^{-1} and 9.8 S m^{-1} for MS and CM samples, respectively. Besides, both

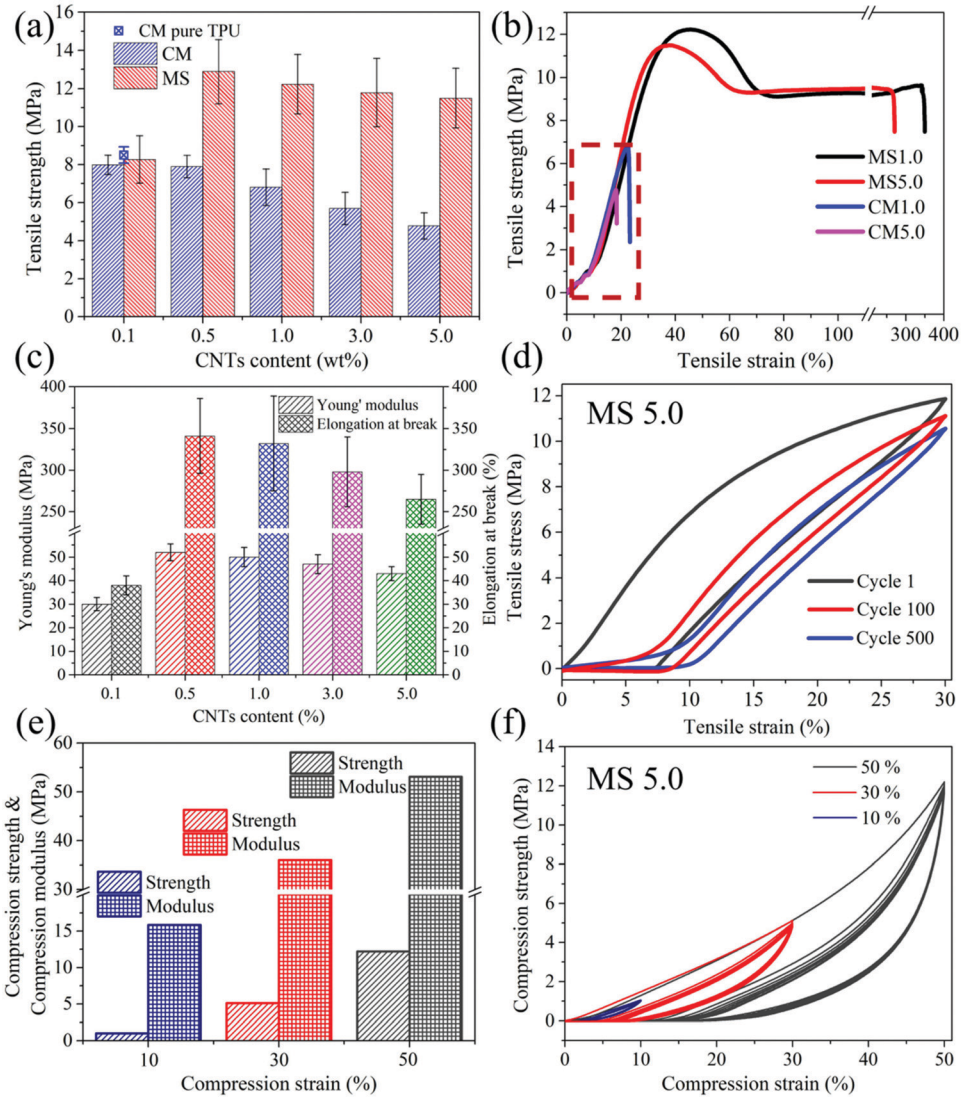

Fig. 4 (a) Tensile strength of the pure TPU prepared by compression molding, CM and MS samples with various CNT contents; (b) typical tensile stress–strain curves of the MS and CM samples with 1.0 wt% and 5.0 wt% CNT; (c) elongation at break and tensile modulus; (d) cyclic stretching-recovery curves of $MS_{5.0}$; (e) compression strength and modulus; (f) cyclic stress–strain curves of $MS_{5.0}$ at various compression strains.

the MS and CM composites showed a percolation behavior, and the following scaling law relationship is used to determine the percolation threshold (φ_c) behaviors. According to the classical percolation theory, σ of a composite material can be described as eqn (5).[41,42]

$$\sigma = \sigma_0(\varphi - \varphi_c)^t \quad (5)$$

where, σ and σ_0 are the conductivity of the composite materials and proportionality constant related to the intrinsic conductivity of the filler, respectively. φ is the volume fraction of the fillers and φ_c is the percolation volume fraction. t is a critical exponent that reflects the system dimensionality of the conductive network.[43] It follows a power-law dependence of approximately 1.6–2 in a three dimensional system, and 1–1.3 in a two dimensional system.[14] The fitted curves are shown in Fig. 5a and the calculated percolation threshold is 0.06 vol% and 0.057 vol% for MS and CM samples, respectively. The low φ_c value obtained in our work is lower than most of the previously reported research.[44–50] In addition, the t value of the MS samples is 2.40, only slightly lower than that of the CM samples (2.51), suggesting that the conductive network of the MS sample is not essentially changed. The low threshold value of our segregated MS composites could be attributed to the selective distribution of CNTs at the interfaces among TPU granules, which increases the effective CNT concentration for constructing the conductive pathways during the microwave selective sintering procedure, along with the perfection of 3D CNT conductive networks. It is exciting that the 2.94 vol% of CNTs leading to an excellent electrical conductivity of 17.9 S m^{-1} of our MS sample far exceeds the target value (1 S m^{-1}) for commercial use.

In many applications, electromechanical durability under repeated stress cycles is an important requirement for elastic and stretchable CPCs.[51] Considering the good mechanical

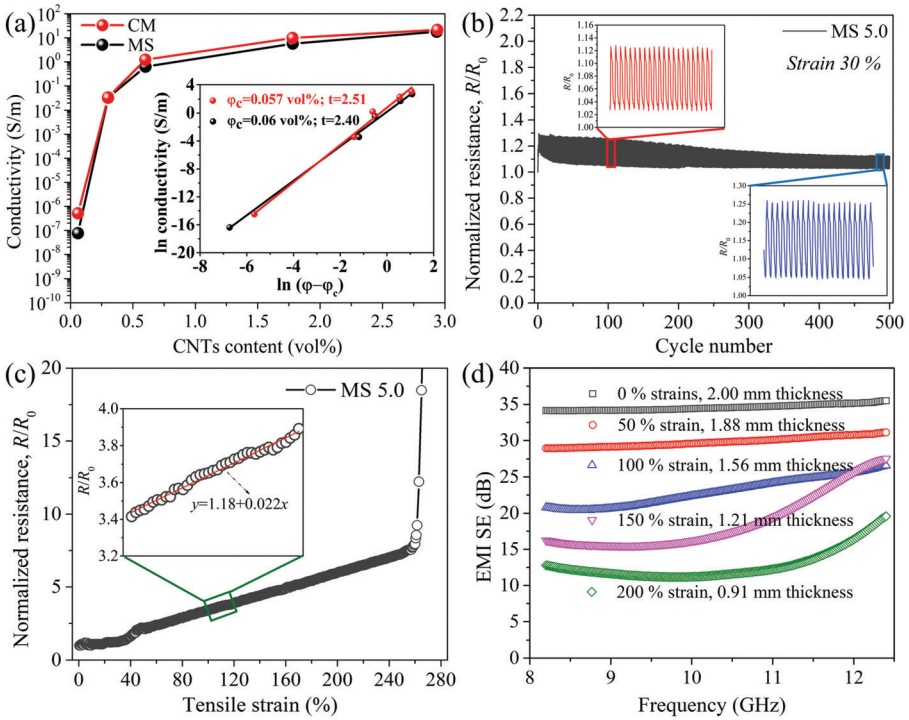

Fig. 5 (a) Electrical conductivity *vs.* CNT content for the MS and CM samples (the inset shows a ln–ln plot of the conductivity *vs.* $\varphi-\varphi_c$, lines correspond to the least square fitting of the experimental data); (b) normalized electrical resistance (R/R_0) of $MS_{5.0}$ under repeated stretching-recovery at a rate of 50 mm min^{-1} with a maximum strain of 30%; (c) normalized electrical resistance (R/R_0) of $MS_{5.0}$ during monotonic tension at a rate of 50 mm min^{-1}; (d) EMI SE of $MS_{5.0}$ at the given strains.

stability and high stretchability of the prepared TPU/CNT composites, a constant external force might induce a regular change in its electrical resistance caused by the deformation of the segregated CNT network. As shown in Fig. S3 (ESI†), the electrical resistance of the sample was recorded in real-time during the stretching process. Fig. 5b shows the changes in the normalized electrical resistance (R/R_0, R and R_0 refer to the resistances during the strain and the initial resistance) of $MS_{5.0}$ during the repeated stretching-recovery process. The consistent resistance variation with stretching force applied on the $MS_{5.0}$ sample can be maintained during hundreds of cycles, making it promising for use as the strain sensor with long working life and reliability. Fig. 5c shows the changes of stress and R/R_0 during stretching with an increase of tensile strain. In general, higher electrical conductivity involves a high-quality conductive network in CPCs, which might result in better stability in the tensile resistance test. In Fig. 5c, the value of R/R_0 increased slowly during the stretching process, even the sample was stretched to a high strain of 250%, indicating the good stability of the CNT conductive network of our $MS_{5.0}$ sample. At the same time, the tensile sensing responsivity R/R_0 shows fantastic linearity along the strain until failure. In the equation (shown), the relative change in R/R_0 to the tensile strain is calculated to be 0.022, the linearity of the sample endows these segregated composites with potential application in the sensor field. Moreover, we recorded the EMI SE values of the $MS_{5.0}$ sample at the given strains, including 50%, 100%, 150%, and 200%, and the related curves were shown in Fig. 5d. In agreement with the change in R/R_0, the EMI SE shows a downtrend with an increase of strain, which could be attributed to the increase in electrical resistance as well as the decrease in thickness of the test samples. For instance, under the strain of 50%, the average EMI SE was reduced to 29.81 dB (1.88 mm) compared to 34.57 dB (2.00 mm) of the unstretched sample. Moreover, it can be seen that the EMI SE of the $MS_{5.0}$ is almost independent of frequency under low strains in the X-band range, revealing the good interaction between CNTs and the TPU matrix. However, it should be noticed that there is a significantly decrease in the average EMI SE, especially for the highly stretched samples (*i.e.*, 12.8 dB under 200% of strain). Meanwhile, the highly stretched samples showed a typical high EMI SE value in the high frequency range (11–12.4 dB). This could be attributed to the electromagnetic waves with a specific wavelength reflecting back and forth in the oriented segregated network caused by high stretching.

3.4 EMI shielding performance

A high EMI shielding property is especially important for CPCs to achieve potential applications in some advanced fields. Fig. 6a shows the EMI SE of the MS composites (2.0 mm in thickness) in the X-band (8.2–12.4 GHz), which is the frequency widely used in telecommunication applications. It showed that the EMI SE of the MS samples shows a weak frequency dependence across the measured range and increases obviously with the CNT content, as a result of the improved electrical conductivity at higher CNT loading. For example, the sample of

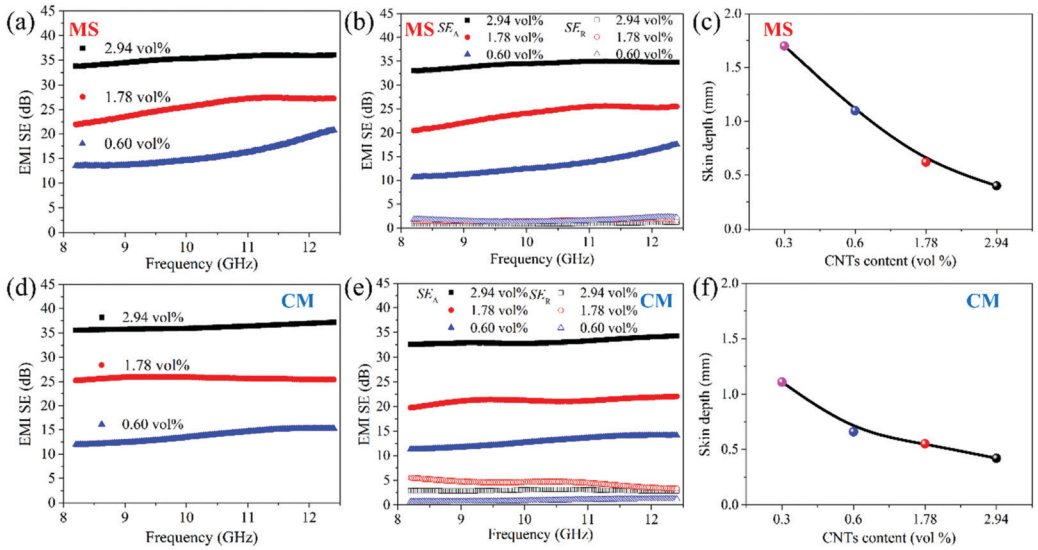

Fig. 6 (a and b) SE_T, SE_A, and SE_R for the MS samples; (c) skin depth of MS *vs.* CNT volume content; (d and e) SE_T, SE_A, and SE_R for the CM samples; (f) skin depth of CM with different CNT volume contents. (The thickness of the sample is 2.0 mm.)

$MS_{3.0}$ and $MS_{5.0}$ showed an average EMI SE of 25.6 and 35.3 dB, respectively, which showed the comparable average EMI SE to the $CM_{3.0}$ (25.7 dB) and $CM_{5.0}$ (36.2 dB) samples (Fig. 6d). The selective distribution of CNTs sharply increased the SE_T which far exceeds the target EMI SE value (20 dB) for commercial use. The SE_T can be defined as the logarithmic ratio of the incident to transmitted power as given in eqn (6):[10]

$$SE_T\ (dB) = 10\lg(P_i/P_t) \quad (6)$$

where P_i is the incident and P_t is transmitted or remaining power in decibels (dB). The blocking of 99% incident microwave energy is required to meet the practical application (20 dB) in EMI shielding devices. As expected, the SE_T values of the MS samples reveal that only 0.28 to 0.03% of electromagnetic radiation can transmit through the shielding materials. Table S1 (ESI†) showed the comparison of the EMI SE of our MS samples with that of polymer nanocomposites which have been reported in the literature.[12,15,17,19,20,55–60] The excellent EMI SE achieved by our MS techniques was superior to that of conventional CPCs, along with improved mechanical performance. In addition, the obtained EMI SE performance of our MS samples is comparable to the reported segregated CPCs.

To explore the EMI shielding mechanism in MS samples, SE_R and SE_A at a X-band frequency were calculated from scattering parameters, as shown in Fig. 6b, it is obvious that the contribution of SE_A to the total SE_T is much larger than SE_R, which confirms that the microwave absorption of electromagnetic waves plays a major role in the MS samples rather than the reflection mechanism.[52] Besides, the CM composites showed a similar microwave absorption mechanism (Fig. 6e).

Skin depth, δ, is an important parameter for the evaluation of the shielding ability of the materials. It represents the depth at which the intensity of the radiation inside the material decreases to $1/e$ of its original value on the surface, and it determines the SE_A values of materials with a fixed thickness, d.[53] According to the classical electromagnetic theory, the absorption effectiveness can be expressed as eqn (7) for CPCs:[46]

$$SE_A\ (dB) = 20\frac{d}{\delta}\log e \quad (7)$$

The skin depth depends on the frequency according to eqn (8).[54]

$$\delta = \frac{1}{\sqrt{\pi f \mu \sigma}} \quad (8)$$

where f is the frequency, σ is the electrical conductivity, and μ is the magnetic permeability of materials (*i.e.* $\mu = \mu_0\mu_r$, where $\mu_0 = 4\pi \times 10^{-7}$ H m^{-1} and μ_r is the material's relative magnetic permeability, and $\mu_r = 1$ for the nonmagnetic TPU/CNT composites). Fig. 6c shows the skin depth of the MS samples at various CNT contents, which is the average value of the investigated 8.2–12.4 GHz frequency range. The curve revealed that the skin depth for our segregated $MS_{5.0}$, $MS_{3.0}$ and $MS_{1.0}$ samples was in 0.42–0.66 mm range, and these values are much smaller than the thickness of the tested sample (2.0 mm), suggesting that the segregated MS composites showed excellent EMI shielding properties. From Fig. 6f, it could be noticed that the CM samples in all CNT contents also showed excellent EMI shielding properties ($\delta < 1.2$ mm). Again, the use of microwave selective sintering reveals a promising strategy to design and develop high-strength segregated CPCs with high EMI shielding performance, which could be applied to various type of polymers, and the corresponding study is underway.

4. Conclusions

In summary, we reported the use of microwave selective sintering to prepare mechanically strong segregated TPU/CNT composites for the first time. CNTs, here, were selectively distributed on the surface of TPU granules *via* a ball milling method.

Upon irradiation, the CNTs (act as a microwave energy absorber) were responsible for a local temperature increase and correspondingly, resulting in CNTs embedded on the TPU grain surface, and the strong interfacial adhesion of TPU granules was facilitated in a self-designed Teflon mold. The unique "welding" mechanism endowed the segregated TPU/CNT composites with significantly enhanced mechanical properties, exhibiting an excellent elongation at break of about 350%, ten times higher than that of the segregated samples prepared by CM. The obtained microwave sintering TPU/CNT composites with 5.0 wt% CNTs showed an excellent conductivity and an EMI SE of 17.9 S m^{-1} and 35.3 dB, respectively. Our current effort sets a smart yet flexible path to integrate efficient EMI shielding with high mechanical performance in segregated CPCs, holding great promise to satisfy the high demand for upcoming electronic devices.

Conflicts of interest

The authors declare no competing interest.

Acknowledgements

This work was support by the National Natural Science Foundation of China (51720105012).

References

1 F. Shahzad, M. Alhabeb, C. B. Hatter, B. Anasori, H. S. Man, C. M. Koo and Y. Gogotsi, *Science*, 2016, **353**, 1137–1140.
2 Y. Chen, H. B. Zhang, Y. Yang, M. Wang, A. Cao and Z. Z. Yu, *Adv. Funct. Mater.*, 2016, **26**, 447–455.
3 W. Song, C. Gong, H. Li, X. D. Cheng, M. Chen, X. Yuan, H. S. Chen, Y. Yang and D. Fang, *ACS Appl. Mater. Interfaces*, 2017, **9**, 1195–1203.
4 M. H. Al-Saleh and U. Sundararaj, *Carbon*, 2009, **47**, 1738–1746.
5 D. X. Yan, H. Pang, B. Li, R. Vajtai, L. Xu, P. G. Ren, J. H. Wang and Z. M. Li, *Adv. Funct. Mater.*, 2015, **25**, 559–566.
6 B. Zhao, C. Zhao, R. Li, S. M. Hamidinejad and C. B. Park, *ACS Appl. Mater. Interfaces*, 2017, **9**, 20873–20884.
7 L. C. Jia, W. J. Sun, C. G. Zhou, D. X. Yan, Q. C. Zhang and Z. M. Li, *J. Mater. Chem. C*, 2018, **6**, 9166–9174.
8 L. C. Jia, Y. K. Li and D. X. Yan, *Carbon*, 2017, **121**, 267–273.
9 F. Qin and C. Brosseau, *J. Appl. Phys.*, 2012, **111**, 061301.
10 S. Yang, W. Li, S. Bai and Q. Wang, *J. Mater. Chem. C*, 2018, **6**, 11209–11218.
11 S. T. Hsiao, C. C. M. Ma, W. H. Liao, Y. S. Wang, S. M. Li, Y. C. Huang, R. B. Yang and W. F. Liang, *ACS Appl. Mater. Interfaces*, 2014, **6**, 10667–10678.
12 M. Arjmand, T. Apperley, M. Okoniewski and U. Sundararaj, *Carbon*, 2012, **50**, 5126–5134.
13 J. Liang, Y. Wang, Y. Huang, Y. Ma, Z. Liu, J. Cai, C. Zhang, H. Gao and Y. Chen, *Carbon*, 2009, **47**, 922–925.
14 J. Du, L. Zhao, Y. Zeng, L. Zhang, F. Li, P. Liu and C. Liu, *Carbon*, 2011, **49**, 1094–1100.
15 H. Pang, L. Xu, D. X. Yan and Z. M. Li, *Prog. Polym. Sci.*, 2014, **39**, 1908–1933.
16 Y. Zhan, J. Wang, K. Zhang, Y. Li, Y. Meng, N. Yan, W. Wei, F. Peng and H. Xia, *Chem. Eng. J.*, 2018, **344**, 184–193.
17 X. P. Zhang, L. C. Jia, G. Zhang, D. X. Yan and Z. M. Li, *J. Mater. Chem. C*, 2018, **6**, 10760–10766.
18 S. Gupta, R. Ou and R. A. Gerhardt, *J. Electron. Mater.*, 2006, **35**, 224–229.
19 M. Yoonessi and J. R. Gaier, *ACS Nano*, 2010, **4**, 7211–7220.
20 W. C. Yu, J. Z. Xu, Z. G. Wang, Y. F. Huang, H. M. Yin, L. Xu, Y. W. Chen, D. X. Yan and Z. M. Li, *Composites, Part A*, 2018, **110**, 230–245.
21 H. Pang, D. X. Yan, Y. Bao, J. B. Chen, C. Chen and Z. M. Li, *J. Mater. Chem.*, 2012, **22**, 23568–23575.
22 T. Li, L. F. Ma, R. Y. Bao, G. Q. Qi, W. Yang, B. H. Xie and M. B. Yang, *J. Mater. Chem. A*, 2015, **3**, 5482–5490.
23 R. R. Mishra and A. K. Sharma, *Composites, Part A*, 2016, **81**, 78–97.
24 M. Zhang, S. Fang, A. A. Zakhidov, S. B. Lee, A. E. Aliev, C. D. Williams, K. R. Atkinson and R. H. Baughman, *Science*, 2005, **309**, 1215–1219.
25 T. Imholt, C. A. Dyke, B. Hasslacher, J. M. Pérez, D. Price, J. A. Roberts, J. Scott, A. Wadhawan, Z. Ye and J. M. Tour, *Chem. Mater.*, 2003, **15**, 3969–3970.
26 C. Wang, T. Chen, S. Chang, S. Cheng and T. Chin, *Adv. Funct. Mater.*, 2007, **17**, 1979–1983.
27 T. Wu, Y. Pan, E. Liu and L. Li, *J. Appl. Polym. Sci.*, 2012, **126**, E283–E289.
28 S. Poyraz, L. Zhang, A. Schroder and X. Zhang, *ACS Appl. Mater. Interfaces*, 2015, **7**, 22469–22477.
29 C. B. Sweeney, B. A. Lackey, M. J. Pospisil, T. C. Achee, V. K. Hicks, A. G. Moran, B. R. Teipel, M. A. Saed and M. J. Green, *Sci. Adv.*, 2017, **3**, e1700262.
30 L. Chen, C. Y. Tang, H. S. L. Ku, C. P. Tsui and X. Chen, *Composites, Part B*, 2014, **56**, 504–511.
31 K. Yu, Y. Liu and J. Leng, *RSC Adv.*, 2014, **4**, 2961–2968.
32 A. Hazarika, B. K. Deka, D. Kim, K. Kong, Y. B. Park and H. W. Park, *Sci. Rep.*, 2017, **7**, 40386.
33 E. Rezvanpanah, S. R. G. Anbaran and E. Di Maio, *Carbon*, 2017, **125**, 32–38.
34 J. Cheng, R. Roy and D. Agrawal, *J. Mater. Sci. Lett.*, 2001, **20**, 1561–1563.
35 X. P. Zhang, L. C. Jia, G. Zhang, D. X. Yan and Z. M. Li, *J. Mater. Chem. C*, 2018, **6**, 10760–10766.
36 F. Shahzad, P. Kumar, S. Yu, S. Lee, Y.-H. Kim, S. M. Hong and C. M. Koo, *J. Mater. Chem. C*, 2015, **3**, 9802–9810.
37 M. Šupová, G. S. Martynková and K. Barabaszová, *Sci. Adv. Mater.*, 2011, **3**, 1–25.
38 W. C. Yu, T. Wang, G. Q. Zhang, Z. G. Wang, H. M. Yin, D. X. Yan, J. Z. Xu and Z. M. Li, *Compos. Sci. Technol.*, 2018, **167**, 260–267.
39 K. Zhang, G. H. Li, L. M. Feng, N. Wang, J. Guo, K. Sun, K. X. Yu, J. B. Zeng, T. Li and Z. Guo, *J. Mater. Chem. C*, 2017, **5**, 9359–9369.
40 Z. Li, Z. Wang, X. Gan, D. Fu, G. Fei and H. Xia, *Macromol. Mater. Eng.*, 2017, **302**, 1700211.

41 H. Pang, C. Chen, B. Yu, J. Chen, J. Xu, J. Lei and Z. M. Li, *Mater. Lett.*, 2012, **79**, 96–99.
42 H. Abbasi, M. Antunes and J. I. Velasco, *Polymers*, 2018, **10**, 348.
43 C. H. Cui, H. Pang, D. X. Yan, L. C. Jia, X. Jiang, J. Lei and Z. M. Li, *RSC Adv.*, 2015, **5**, 61318–61323.
44 Y. H. Kim and W. Li, *J. Cell. Plast.*, 2013, **49**, 131–145.
45 S. Gong, Z. Zhu, J. Li and S. Meguid, *J. Appl. Phys.*, 2014, **116**, 194306.
46 J. F. Gao, Z. M. Li, Q. J. Meng and Q. Yang, *Mater. Lett.*, 2008, **62**, 3530–3532.
47 Q. Liu, J. Tu, W. Xin, W. Yu, W. Zheng and Z. Zhao, *Carbon*, 2012, **50**, 339–341.
48 L. Yue, G. Pircheraghi, S. A. Monemian and I. Manas-Zloczower, *Carbon*, 2014, **78**, 268–278.
49 S. H. Wang, Y. Wan, B. Sun, L. Z. Liu and W. Xu, *Nanoscale Res. Lett.*, 2014, **9**, 522.
50 S. Zhang, L. Lin, H. Deng, X. Gao, E. Bilotti, T. Peijs, Q. Zhang and Q. Fu, *eXPRESS Polym. Lett.*, 2012, **6**, 159–168.
51 Y. Kazemi, A. R. Kakroodi, A. Ameli, T. Filleter and C. B. Park, *J. Mater. Chem. C*, 2018, **6**, 350–359.
52 K. Zhang, H. O. Yu, Y. D. Shi, Y. F. Chen, J. B. Zeng, J. Guo, B. Wang, Z. Guo and M. Wang, *J. Mater. Chem. C*, 2017, **5**, 2807–2817.
53 F. Sharif, M. Arjmand, A. A. Moud, U. Sundararaj and E. P. Roberts, *ACS Appl. Mater. Interfaces*, 2017, **9**, 14171–14179.
54 Y. Zhan, M. Oliviero, J. Wang, A. Sorrentino, G. G. Buonocore, L. Sorrentino, M. Lavorgna, H. Xia and S. Iannace, *Nanoscale*, 2019, **11**, 1011–1020.
55 B. Sourav, K. Goutam Prasanna and B. Suryasarathi, *ACS Appl. Mater. Interfaces*, 2015, **7**, 25448–25463.
56 Z. Liu, B. Gang, H. Yi, Y. Ma, D. Feng, F. Li, T. Guo and Y. Chen, *Carbon*, 2007, **45**, 821–827.
57 K. Levon, A. Margolina and A. Z. Patashinsky, *Macromolecules*, 1993, **26**, 4061–4063.
58 M. Arjmand, M. Mahmoodi, G. A. Gelves, S. Park and U. Sundararaj, *Carbon*, 2011, **49**, 3430–3440.
59 S. Deng, Y. Zhu, X. Qi, W. Yu, F. Chen and Q. Fu, *RSC Adv.*, 2016, **6**, 45578–45584.
60 H. B. Zhang, W. G. Zheng, Q. Yan, Z. G. Jiang and Z. Z. Yu, *Carbon*, 2012, **50**, 5117–5125.